

Skyrmions in a magnetic field and π^0 domain wall formation in dense nuclear matter

Shi Chen, Kenji Fukushima, and Zebin Qiu
Department of Physics, The University of Tokyo,
7-3-1 Hongo, Bunkyo-ku, Tokyo 113-0033, Japan

We elucidate magnetic effects in the Skyrmion system to probe into the dense nuclear matter. We find a deformed π^0 dipole structure of a Skyrmion and quantify nontrivial rearrangements of the confining pressure distribution. We confirm an isospin-dependent baryon spectrum from the anomaly-induced action. We then extend our scope to stacked Skyrme Crystal layers to scrutinize phases of magnetized nuclear matter. We observe a quantized magnetic flux and identify a phase transition from a crystalline state to a π^0 domain wall corresponding to a topological transmutation from $\pi_3(S^3)$ to $\pi_1(S^1)$. We establish the phase diagram, which could be explored also in analogous systems with two-component Bose-Einstein condensates.

Introduction: It is of paramount importance to deepen our understanding of dense baryonic matter. The phase diagram of matter out of quarks and gluons has not been established due to the sign problem of the Monte-Carlo algorithm in quantum chromodynamics (QCD) at finite density. The beam energy scan program of the relativistic heavy-ion collision (see [1, 2] for recent highlights) aims to unveil properties of dense matter and prompt next-generation approaches; see [3–6] for theoretical and phenomenological attempts. Besides the heavy-ion collision, the structure of neutron stars and the dynamics of the neutron star merger crucially depend on the equation of states of dense matter. Numerous endeavors are devoted to constrain properties of dense matter by the extrapolation from the low-density nuclear matter and/or the high-density quark matter, as well as the interpolation between them; see [7, 8] for reviews.

Given the lack of available persuasive constraints, it is beneficial to incorporate additional parameter dimensions. An intriguing candidate is a strong magnetic background, which emerges as a gigantic magnetic pulse in non-central collisions (see [9] for a discussion and [10] for a review), and also penetrates from the neutron star surface into its deep core. It would be a milestone to identify the ground state of dense matter in the strong magnetic field limit. Interestingly, the sign problem in such a system may be moderate as pointed out in [11] and further studied with a two-color QCD benchmark test in [12]. A promising candidate of quark matter is an inhomogeneous state called the Chiral Magnetic Spiral [13], which is analogous to a Quarkyonic Spiral as proposed in [14] and modeled in [15]. The Quarkyonic Spiral shares the same physical properties with the dual chiral density wave state [16] whose nuclear counterpart is the P -wave pion condensate [17]. Recent analyses of the Chiral Lagrangian have further bespoken a novel scenario of the Chiral Soliton Lattice (CSL) [18, 19], which crystallizes inhomogeneous π^0 configurations in a way similar to the π^0 domain wall addressed in [19] (see also [20]). There are many studies based on effective models for magnetized quark matter (e.g., [21]), while the magnetic responses of nuclear matter are to be explored.

Unlike quark matter, nuclear matter does not involve intricate ultraviolet degrees of freedom such as gluons and quarks, which justifies the applicability of infrared effective theories. As the predominant infrared physics of QCD, the chiral symmetry breaking realizes baryon symmetry topologically by $\pi_3(\text{SU}(2))$ [22]. A magnetic field devotes an additional axial $\pi_1(\text{U}(1))$ contribution. Thus from the infrared viewpoint, we rephrase the competition between the above two scenarios as the duel between two topological realizations of baryon symmetry, i.e., $\pi_3(\text{SU}(2))$ vs. $\pi_1(\text{U}(1))$. Such topological interference is interesting on its own and also applicable in other circumstances such as the two-component Bose-Einstein condensation [23].

It is natural to identify the solitons under the baryon symmetry as the baryons, which proves rigorous in the large- N_c (color) limit [24]. We therefore employ the Skyrme model [25–27] to investigate various scenarios of dense nuclear matter under a strong magnetic background; see [28] for a related review. We notice that an *ad hoc* interplay between the CSL and the Skyrme Crystals was previously discussed in [29] but we will clarify a self-consistent mechanism for the CSL formation out of dense nuclear matter via the Skyrme Crystals. Finally, we will present the phase diagram of magnetized nuclear matter belonging to different homotopy groups.

Skyrmions with electromagnetism: In Chiral Effective Theory, infrared degrees of freedom generated by the spontaneous breaking of (approximate) chiral symmetry are embodied by $\Sigma = e^{i\pi\cdot\tau/f_\pi} \in \text{SU}(N_f)$ where N_f is the flavor number and π represents the (pseudo) Nambu-Goldstone bosons. The infrared amplitude of π is reproduced by a quadratic action plus a mass term:

$$S_0 = -\frac{f_\pi^2}{4} \int d^4x \left[\text{tr}(\ell_\mu \ell^\mu) + 2m_\pi^2 \text{tr}(1-\Sigma) \right], \quad (1)$$

where $\ell_\mu \equiv \Sigma^\dagger D_\mu \Sigma$ with the covariant derivative $D_\mu \Sigma \equiv \partial_\mu \Sigma - iA_\mu[Q, \Sigma]$ for an electric charge $iQ \in \mathfrak{u}(N_f)$. The elementary charge e is absorbed in the gauge field A_μ in our convention. The 't Hooft anomalies are matched by the Wess-Zumino-Witten action, S_{WZW} [30, 31], and

$\pi_3(\text{SU}(N_f))$ -induced topological symmetry is recognized as baryon $\text{U}(1)_B$ [22].

In the Skyrme model that treats solitons protected by this symmetry, to evade Derrick's scaling theorem [32], a higher-derivative term,

$$S_{\text{Sky}} = \frac{1}{32a^2} \int d^4x \text{tr} \left([\ell_\alpha, \ell_\beta] [\ell^\alpha, \ell^\beta] \right), \quad (2)$$

is added. Dimensionless variables rescaled by f_π and a will be used for our results. The chiral limit, i.e., $m_\pi = 0$, is taken throughout this paper for simplicity.

Gauging the $\mathfrak{su}(N_f)$ sector appropriately, we see that the covariant derivative is blind to the $\mathfrak{u}(1)_B$ sector of Q , which claims an extra coupling, $S_B = q \int d^4x A_\mu J_B^\mu$ with $q \equiv \frac{N_c}{N_f} \text{tr} Q$ and

$$j_B^\mu = \frac{1}{24\pi^2} \epsilon^{\mu\nu\alpha\beta} \left\{ \text{tr}(\ell_\nu \ell_\alpha \ell_\beta) + i \frac{3}{2} F_{\alpha\beta} \text{tr}[Q(\ell_\nu - \bar{\ell}_\nu)] \right\} \quad (3)$$

where we denote $\bar{\ell}_\mu \equiv \Sigma D_\mu \Sigma^\dagger$ and $\epsilon_{0123} = -\epsilon^{0123} = 1$.

In this work, we intently treat the case of $N_f = 2$. Then S_{WZW} is simply a \mathbb{Z}_2 θ -angle from $\pi_4(\text{SU}(2))$, which is nontrivial for odd N_c , agglutinating $\text{U}(1)_B$ to other transformations via the fermionic statistics [22]. For $N_c = 3$, the physical charge $Q = \text{diag}(\frac{2}{3}, -\frac{1}{3})$ breaks isospin-symmetry to I_3 -generated axial iso-rotation. We introduce a homogeneous downward magnetic field $\mathbf{B} = -B\hat{z}$ with $B \geq 0$, adopting $A_0 = 0$ and $\mathbf{A} = \frac{1}{2}B\mathbf{r} \times \hat{z}$ in the symmetric gauge.

Skyrmion deformed by a magnetic field: We adopt a general Ansatz for a (classical) static Skyrmion, i.e., the *axial hedgehog Ansatz*, on account of the pseudo-axial symmetry, $\Sigma(\mathbf{r}e^{i\alpha\hat{z}}) = e^{i\alpha Q} \Sigma(\mathbf{r}) e^{-i\alpha Q}$. Parametrizing $\Sigma = i\boldsymbol{\tau} \cdot \boldsymbol{\Pi} + \Pi_4$ as

$$\begin{aligned} \Pi_1 &= \sin f \sin g \cos \varphi, & \Pi_3 &= \sin f \cos g, \\ \Pi_2 &= \sin f \sin g \sin \varphi, & \Pi_4 &= \cos f, \end{aligned} \quad (4)$$

we can conveniently express the axial hedgehog as

$$f = f(r, \theta), \quad g = g(r, \theta), \quad \varphi = \varphi_0(r, \theta) + \phi, \quad (5)$$

within the spherical coordinates (r, θ, ϕ) . The request of a unit baryon number stipulates boundary conditions: $f(\infty, \theta) = 0$, $f(0, \theta) = \pi$, $g(r, 0) = 0$, $g(r, \pi) = \pi$. En passant, the celebrated spherical hedgehog [27] is recovered provided $f = f(r)$, $g = \theta$, and $\varphi = \phi$.

The static Euler-Lagrange equation minimizes the energy functional $M(f, g, \varphi_0)$, i.e., the spatial integral of T^{00} , with $T^{\mu\nu}$ the energy-stress tensor. Our Ansatz gives $M = 2\pi \int_0^\infty dr r^2 \int_{-1}^1 d\cos\theta T^{00}(r, \theta)$ with

$$\begin{aligned} T^{00} &= \frac{f_\pi^2}{2} \left\{ |\nabla f|^2 + \sin^2 f \left[|\nabla g|^2 + \sin^2 g (\Upsilon^2 + |\nabla \varphi_0|^2) \right] \right\} \\ &+ \frac{1}{2a^2} \sin^2 f \left\{ |\nabla f \times \nabla g|^2 + \sin^2 g \left[\Upsilon^2 (|\nabla f|^2 + \sin^2 f |\nabla g|^2) \right. \right. \\ &\left. \left. + |\nabla f \times \nabla \varphi_0|^2 + \sin^2 f |\nabla g \times \nabla \varphi_0|^2 \right] \right\}, \end{aligned} \quad (6)$$

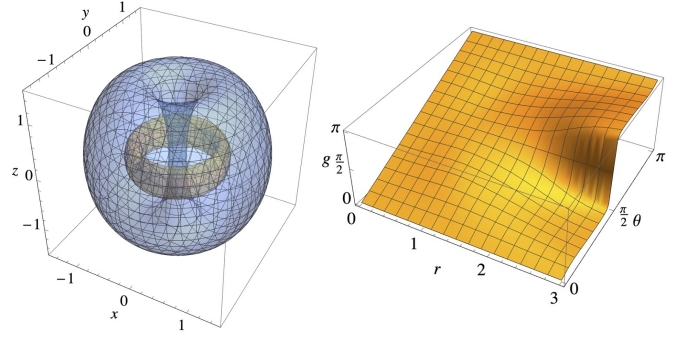


FIG. 1. (Left) Graphical representation of $\pi_3(\text{SU}(2))$ with $B = 3.00f_\pi^2 a^2$; $\Pi_1^2 + \Pi_2^2 = 0.90$ on the inner torus (orange) and $\Pi_3^2 + \Pi_4^2 = 0.90$ on the outer torus (blue). (Right) $g(r, \theta)$ with $B = 3.00f_\pi^2 a^2$. (x, y, z and r are of unit $f_\pi^{-1}a^{-1}$.)

where $\Upsilon \equiv \frac{1}{r \sin \theta} - \frac{Br \sin \theta}{2}$. We note $|\nabla h|^2 = (\partial_r h)^2 + \frac{1}{r^2} (\partial_\theta h)^2$ and $|\nabla h \times \nabla w|^2 = \frac{1}{r^2} (\partial_r h \partial_\theta w - \partial_\theta h \partial_r w)^2$ for any functions $h(r, \theta)$ and $w(r, \theta)$.

A uniform $\varphi_0(r, \theta)$ is necessary to minimize the energy functional quadratic in $\nabla \varphi_0$. Then employing the finite element method, we solve the Dirichlet problem of only two functions, $f(r, \theta)$ and $g(r, \theta)$, from two equations of motion, $\delta M / \delta f = 0$ and $\delta M / \delta g = 0$, with the boundary conditions prescribed below Eq. (5). Figure 1 shows how the spatial profile of our solution maintains a topological winding at finite $B = 3.00f_\pi^2 a^2$. The orange inner and the blue outer tori in Fig. 1 (Left) represent surfaces of $\Pi_1^2 + \Pi_2^2 = 0.90$ and $\Pi_3^2 + \Pi_4^2 = 0.90$ respectively. It is evident that the inner torus is laced with a brace from the outer torus, which is a graphical representation of $\pi_3(\text{SU}(2))$ winding; see also Ref. [23]. Besides, as shown in Fig. 1, our numerical solutions turn out to satisfy

$$f(r, \pi - \theta) = f(r, \theta), \quad g(r, \pi - \theta) = \pi - g(r, \theta). \quad (7)$$

Uniform φ_0 and Eq. (7) show pseudo-reflection symmetry which will play a role in the treatment below Eq. (10).

Magnetic effects are characterized by a virtual ‘‘barrel’’ whose wall locates at $\Upsilon = 0$, i.e., $r \sin \theta = \sqrt{2/B}$. To minimize the potential term $\Upsilon^2 \sin^2 f \sin^2 g = \Upsilon^2 (\Pi_1^2 + \Pi_2^2)$ in the energy functional, $\Pi_{1,2}$ tend to inhabit the barrel wall. For weak $B \lesssim 0.4f_\pi^2 a^2$, a broad barrel mildly expands the Skyrmion profile transversely (i.e., *oblate deformation*). In contrast, for strong $B \gtrsim 0.4f_\pi^2 a^2$, constricted by a narrow barrel, the profile shrinks drastically, especially in transverse directions (i.e., *prolate deformation*), as shown in Fig. 1 (Left). Actually, since the B -term dominates $\Upsilon < 0$, the exterior $\Pi_{1,2}$ is radically suppressed, as shown by the angular distortion of $g(r, \theta)$ in Fig. 1 (Right). We witness a sharp leap from $g \sim 0$ to π near $\theta = \frac{\pi}{2}$ for $r \gtrsim \sqrt{2/B}$, inferring that the Skyrmion pulls its π^\pm cloud in and leaves a sheer π^0 dipole outside. It is then natural to conjecture that transversely contiguous π^0 dipoles will condense into a π^0 domain wall, as we shall discuss later.

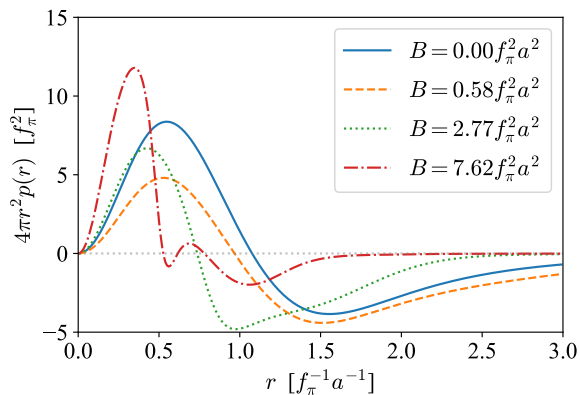


FIG. 2. Pressure distribution at $\theta = \pi/2$ for various B .

The barrel physics is also quantified by the Lorentz force on electric current \mathbf{j}_Q . We found a circumfluence right-handed to \mathbf{B} inside the barrel and a left-handed one outside. The net overall effect of the Lorentz force is captured by the magnetic moment $\mathbf{m} \equiv \int d^3x \frac{1}{2} \mathbf{r} \times \mathbf{j}_Q$ via a pressure sum rule,

$$\int d^3x p(\mathbf{r}) = -\frac{2}{3} \mathbf{m} \cdot \mathbf{B}, \quad (8)$$

derived from $\partial^\mu T_{\mu\nu} = j_Q^\alpha F_{\alpha\nu}$. The right hand side of Eq. (8) is encoded in the Skyrmion mass through $dM = -\mathbf{m} \cdot d\mathbf{B}$. $M(B)$ is evaluated numerically to consist of an expected descent and a subsequent increase, featuring a minimum $M(B_0) = 59.6 f_\pi a^{-1}$ at $B_0 = 2.77 f_\pi^2 a^2$ [whereas $M(0) = 72.9 f_\pi a^{-1}$]. This non-monotonicity implies that, starting with zero at $B = 0$, $\int d^3x p$ gets negative for $0 < B < B_0$ and turns positive for $B > B_0$. To elaborate this behavior we illustrate in Fig. 2 the transverse distribution of $p(\mathbf{r})$ for four characteristic values of B : 0, $0.58 f_\pi^2 a^2$ (where $\int d^3x p$ is minimized), $2.77 f_\pi^2 a^2$ (B_0), and $7.62 f_\pi^2 a^2$ (where $|\mathbf{m}|$ in $B > B_0$ is maximized). Based on these expositions we propose that a weak B produces a liberating force, while a strong B stimulates a confining force.

Nucleon as a quantized Skyrmion: To distinguish protons from neutrons, we seek isospin eigenstates by varying the static solution as $\Sigma(t) = e^{i\alpha(t)Q} \Sigma e^{-i\alpha(t)Q}$. The Lagrangian then reads, $\mathcal{L} = \frac{1}{2} \Gamma \dot{\alpha}^2 - \Phi \dot{\alpha} - M$, with $\Gamma = \int d^3x \sin^2 f \sin^2 g [f_\pi^2 + \frac{1}{a^2} (|\nabla f|^2 + |\nabla g|^2 \sin^2 f)]$, $\Phi = \frac{gB}{4\pi^2} \int d^3x \sin \theta \sin^2 f \sin g (\partial_\theta f \partial_r g - \partial_r f \partial_\theta g)$, and M being the classical mass discussed above. Introducing the canonical momentum, $\beta \equiv \delta S / \delta \dot{\alpha} = \dot{\alpha} \Gamma - \Phi$, we write down the Hamiltonian via the Legendre transformation:

$$H = \beta \dot{\alpha} - \mathcal{L} = M + \frac{1}{2\Gamma} (\beta + \Phi)^2. \quad (9)$$

The 2π -periodicity of $\alpha(t)$ with the \mathbb{Z}_2 θ -angle assigns a half-odd-integer spectrum to β . Invoking the pseudo-axial symmetry of our Ansatz, Noether's theorem informs

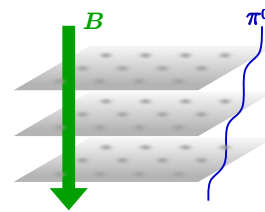


FIG. 3. Schematic illustration of the Chiral Soliton Lattice (CSL) as approximated by the 2D Skyrme Crystal layers.

us of $J_3 = -I_3 = \beta$. Confirming $\Phi(B) \geq 0$ numerically, we conclude that the ground state is a spin-down proton $|p\downarrow\rangle$, and the lowest excitation is a spin-up neutron $|n\uparrow\rangle$. We also verify that the masses of both nucleons, $\langle p\downarrow | H | p\downarrow \rangle$ and $\langle n\uparrow | H | n\uparrow \rangle$, vary with B in an analogous manner to $M(B)$. Therefore, for weak B our result is consistent with experimental facts that $g_p > 0$, $g_n < 0$, and $|g_p| > |g_n|$. Furthermore, we highlight the general validity of our mass split formula, $m_n - m_p = \Phi/\Gamma$, deduced from Eq. (9), especially for strong B .

We note that M and Γ originate from $S_0 + S_{\text{Sky}}$, while Φ results from S_B solely. Hence, the mass split is in essence an effect of S_B which is muted in the classical static equations of motion. An illuminating explanation hinges on the discrete symmetry $\mathcal{T} e^{i\pi I_2} : \Sigma(t) \rightarrow \Sigma(-t)$ preserved by $S_0 + S_{\text{Sky}}$ but violated by S_B . Since $\mathcal{T} e^{i\pi I_2}$ reverses I_3 and J_3 simultaneously, if we did not gauge the $u(1)_B$ sector of Q via S_B , protons and neutrons would perform remain degenerated.

Domain wall formation from a Skyrme Crystal: Now we come to the most interesting question of the π^0 domain wall formation. As argued in [18] dense nuclear matter under a strong magnetic field may exhibit the CSL, which is approximately viewed as stacked layers of the π^0 domain walls perpendicular to \mathbf{B} as illustrated in Fig. 3. Other phase candidates [16, 17] also exhibit a multilayer structure on account of the anisotropy induced by \mathbf{B} . Hereafter we shall simplify the problem by focusing on a single 2D layer.

We follow the prescription in [33] to actualize a static 2D Skyrme Crystal on a square lattice with pseudo-periodicity that blends crystalline translations with $e^{i\pi I_3}$. We note that, in the presence of the vector potential, crystalline translation should incorporate appropriate gauge transformations, i.e.,

$$\begin{aligned} \tau^3 \Sigma(x, y, z) \tau^3 &= e^{i\lambda B y Q} \Sigma(x+2\lambda, y, z) e^{-i\lambda B y Q}, \\ \tau^3 \Sigma(x, y, z) \tau^3 &= e^{-i\lambda B x Q} \Sigma(x, y+2\lambda, z) e^{i\lambda B x Q}, \end{aligned} \quad (10)$$

where we introduced the lattice constant 2λ . We set one baryon in each unit cell. By imposing pseudo-reflection symmetry $\tau^1 \Sigma(x) \tau^1 = \Sigma^\dagger(-x)$, $\tau^2 \Sigma(y) \tau^2 = \Sigma^\dagger(-y)$, and $\tau^3 \Sigma(z) \tau^3 = \Sigma^\dagger(-z)$ [motivated by the message below Eq. (7)], we can focus on a partial cell with $0 \leq x \leq \lambda$, $0 \leq y \leq \lambda$, and $z \geq 0$. The solution in this octant

cell is subject to a series of boundary conditions. The first is our vacuum convention: $\Pi_4(x, y, +\infty) = 1$. Next, the pseudo-reflection requires $\Pi_1(0, y, z) = \Pi_2(x, 0, z) = \Pi_3(x, y, 0) = 0$. Then, the joint of the pseudo-reflection and the pseudo-translation (10) dictates

$$\begin{aligned} \Pi_1(\lambda, y, z) \sin(\tfrac{1}{2}\lambda B y) - \Pi_2(\lambda, y, z) \cos(\tfrac{1}{2}\lambda B y) &= 0, \\ \Pi_1(x, \lambda, z) \cos(\tfrac{1}{2}\lambda B x) - \Pi_2(x, \lambda, z) \sin(\tfrac{1}{2}\lambda B x) &= 0. \end{aligned} \quad (11)$$

Finally, the octant cell should contain $\frac{1}{8}$ baryon. We recast the baryon number, $N_B \equiv \int d^3x j_B^0 = \frac{1}{4\pi^2} \int (d\varphi - A) \wedge (\Pi_4 d\Pi_3 - \Pi_3 d\Pi_4)$, as a formal surface integral. Foregoing conditions force it to vanish except on two edges. One edge at $x = y = 0$ contributes $N_0 = \frac{1}{8}n_0$, while another at $x = y = \lambda$ yields $N_\lambda = \frac{1}{8}n_\lambda(\frac{2}{\pi}\lambda^2 B - 1)$, where $n_{0,\lambda} \in \mathbb{Z}$ denotes the $\Pi_{3,4}$ winding number from $z = +\infty$ to $-\infty$ along the according edge.

There are two distinct classes of solutions. For the first class which we refer to as the *Normal Crystal*, $N_B = N_0 + N_\lambda = \frac{1}{8}$ for unconstrained λ and B demands $n_0 = 1$ and $n_\lambda = 0$. This completes our list of boundary conditions with $\Pi_4(0, 0, 0) = -1$ and $\Pi_4(\lambda, \lambda, 0) = 1$, which signify a *regional* π^0 domain wall configuration. Then prescribing boundary conditions above, we formulate a Dirichlet problem in the octant cell by minimizing the energy functional $M(\Pi_{1,2,3,4})/8$ with a Lagrange multiplier that constrains $\sum_{i=1}^4 \Pi_i^2 = 1$, where

$$\frac{M}{8} = \int d^3x \left(\frac{f_\pi^2}{2} |\mathbf{D}\Pi_i|^2 + \frac{1}{4a^2} |\mathbf{D}\Pi_i \times \mathbf{D}\Pi_j|^2 \right), \quad (12)$$

We note that $\mathbf{D}\Pi_1 = \nabla\Pi_1 - \mathbf{A}\Pi_2$ and $\mathbf{D}\Pi_2 = \nabla\Pi_2 + \mathbf{A}\Pi_1$. Numerical solutions through the finite element method manifest a stable crystalline structure for any $B \geq 0$. In Fig. 4 we plot the crystalline baryon mass M as a function of the specific transverse area $\Lambda \equiv 4\lambda^2$ under different B . The crystalline stability is substantiated by the existence of an energy minimum at $\Lambda = \Lambda_0$ and the asymptotic recovery to the isolated classical mass. By numerical evaluation, we found that the specific binding energy, $M(\infty) - M(\Lambda_0)$, grows monotonically with increasing B , from $6.40f_\pi a^{-1}$ at $B = 0$ up to a saturated value $\sim 30f_\pi a^{-1}$ for large B . Such magnetically facilitated crystallization confirms our conjectured mechanism of the π^0 -dipole condensation.

The second class of solutions, dubbed the *Anomalous Crystal*, is subject to a constraint, $4\lambda^2 B = 2\pi$. Since such a constraint enforces $N_\lambda = 0$ regardless of n_λ , we remove $\Pi_4(\lambda, \lambda, 0) = 1$ from our list of boundary conditions. Interestingly, we recognize that a transversely uniform π^0 domain wall with $\Pi_4(x, y, 0) = -1$ solves the Anomalous Crystal. Thus our Anomalous Crystal turns out to be a synonym of the conventional *global* π^0 domain wall [19].

Thermodynamics and phase transition: There is a crucial distinction between the two types of 2D crystals.

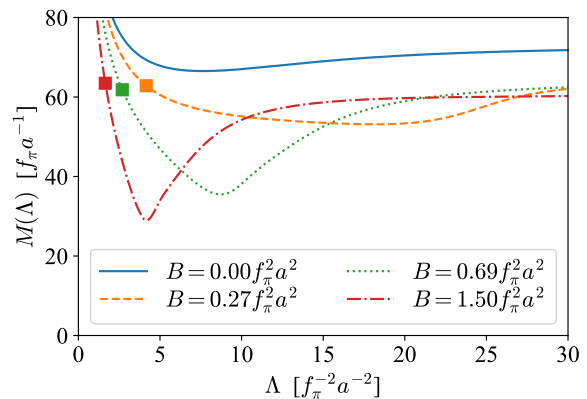


FIG. 4. Crystalline baryon mass $M(\Lambda)$ for various B . The square dots denote the location of Λ_c .

In thermodynamics, our solutions correspond to crystals at $T = 0$ and thus M equals to the free energy per baryon, denoted by \mathcal{E} . For an N -baryon Normal Crystal, the total Helmholtz free energy $F(T, B, N, N\Lambda) \equiv N\mathcal{E}(T, B, \Lambda)$ yields canonical quantities such as the intralayer pressure $\sigma \equiv -(\partial F/\partial(N\Lambda))_{T,B,N} = -(\partial\mathcal{E}/\partial\Lambda)_{T,B}$ and the chemical potential $\mu \equiv (\partial F/\partial N)_{T,B,N\Lambda} = \mathcal{E} + \sigma\Lambda$. In contrast, for an N^* -baryon Anomalous Crystal, the constraint $\Lambda^* = 2\pi/B$ eliminates one degree of freedom, $F^*(T, B, N^*) \equiv N^*\mathcal{E}^*(T, B)$. We use “*” for quantities of the Anomalous Crystal. The Anomalous Crystal is incompressible at a fixed B ; hence we cannot define “*” counterparts of σ and μ .

At fixed T and B , the phase equilibrium of the two distinct crystals should minimize the total Helmholtz free energy, provided the conservation of the total baryon number and area, i.e.,

$$\delta(F + F^*)|_{T,B,N+N^*,N\Lambda+N^*\Lambda^*} = 0. \quad (13)$$

Specifically, we have $\delta F = \mu\delta N - \sigma\delta(N\Lambda)$ and $\delta F^* = \mathcal{E}^*\delta N^*$. There turns out only one independent variation, i.e., $\delta(F + F^*) = (\mu - \sigma\Lambda^* - \mathcal{E}^*)\delta N$. Plugging explicit expressions of σ and μ , we ultimately arrive at the equilibrium criterion:

$$\mathcal{E} - \mathcal{E}^* = (\Lambda - \Lambda^*)\mathcal{E}', \quad (14)$$

where \mathcal{E}' is a shorthand for $(\partial\mathcal{E}/\partial\Lambda)_{T,B}$. Let us define Λ_c as the critical Λ that satisfies Eq. (14). A geometrical approach to locate Λ_c is to find the tangent of $\mathcal{E}(\Lambda)$ that crosses $(\Lambda^*, \mathcal{E}^*)$, yielding Λ_c as the abscissa of the tangential point. To evaluate Λ_c concretely, we quote that $\mathcal{E}^* = 16\pi f_\pi^2 m_\pi/B$ [19] vanishes in the chiral limit and we have identified $\mathcal{E}(\Lambda) = M(\Lambda)$. The shape of $M(\Lambda)$ -curves, with a repulsive core at small Λ , ensures the existence of Λ_c for any $B > 0$. In Fig. 4, we pinpoint the according Λ_c by a square dot on each $M(\Lambda)$ -curve.

In Fig. 5, we plot numerically obtained $\Lambda_c(B)$ and $\Lambda_0(B)$, along with $\Lambda^* = 2\pi/B$. The gradual adherence

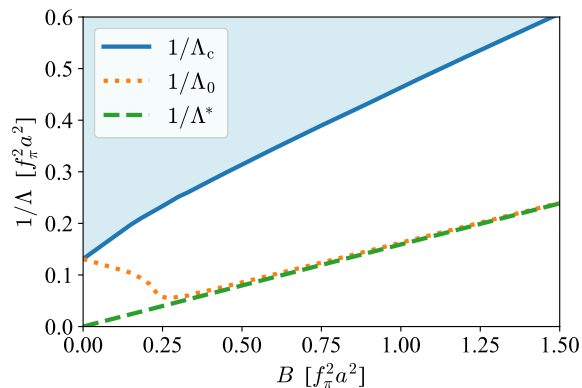


FIG. 5. Numerical results for Λ_c and Λ_0 together with $\Lambda^* = 2\pi/B$ as functions of B . In the (blue) region above $1/\Lambda_c$ the Normal Crystal is favored, while the Anomalous Crystal appears on the (green) dash line of $1/\Lambda^*$.

of $\Lambda_0(B)$ to Λ^* signifies that in general a crystalline “Dirac quantization” (i.e., a quantized magnetic flux) is energetically favored. Figure 5 serves as a phase diagram on the B - Λ^{-1} plane, i.e., the magnetic field versus the baryon (area) density. The Normal Crystal manifests itself as a dense high-pressure phase for $\Lambda^{-1} \geq \Lambda_c^{-1}$ indicated by the blue shaded region in Fig. 5, while the Anomalous Crystal emerges on the line of Λ^* with incompressibility. The former phase principally realizes a $\pi_3(\text{SU}(2))$ winding and the latter exhibits a $\pi_1(\text{U}(1))$ winding exclusively. The two phases are separated by a first-order phase transition, the strength of which is characterized by latent heat. We numerically verify that the specific latent heat, $\mathcal{E}(\Lambda_c) - \mathcal{E}^*$, remains finite with a minimum $61.8f_\pi a^{-1}$ at $B = 0.69f_\pi^2 a^2$, as shown by the green dot in Fig. 4. We will report more about our numerical observations in a full-length paper.

Summary and outlooks: We initially investigated an isolated Skyrmion in a magnetic field. We portrayed an elliptic deformation, unraveled the interplay between confinement and magnetism, and clarified a magnetized baryon spectrum. We subsequently probed into the interaction between magnetically deformed Skyrmions by formulating two types of 2D Skyrme Crystals: a *Normal Crystal* realizes a regional π^0 domain wall, while an *Anomalous Crystal* exhibits a uniform π^0 winding. We established the phase diagram of 2D Skyrme Crystals under careful treatments of thermodynamics.

Lower dimensional crystals put reasonable implications on the realistic 3D dense nuclear matter. Stacked Normal Crystals incarnate inhomogeneous nuclear matter (such as the P -wave π^0 condensate, the dual chiral density wave, etc), while a stack of Anomalous Crystals embodies the CSL phase despite the absence of an anomalous term with a chemical potential. (In our approach, the existence of an anomalous B -term in the baryon

current suffices for this realization.) Granted that longitudinal degrees of freedom bring complications, the equilibrium criteria still include a piece, $\mu - \sigma\Lambda^* - \mathcal{E}^* = 0$, with appropriate prescriptions. Therefore, our 2D analysis proposes a constraint on the CSL phase; it is thermodynamically favored only at relatively low density, and the ordinary nuclear matter would take over the ground state in the higher density region. In other words, for a fixed (volume) density, a larger B would be needed to favor the CSL state. Interesting future works should include the 3D analysis. And a holographic QCD model as argued in [34] may help nonperturbative refinements.

The authors thank Xu-Guang Huang, Mannque Rho, and Naoki Yamamoto for valuable comments and discussions. This work was supported by Japan Society for the Promotion of Science (JSPS) KAKENHI Grant Nos. 18H01211, 19K21874 (KF), and No. 20J20974 (ZQ).

-
- [1] G. Odyniec (STAR), *PoS CORFU2018*, 151 (2019).
 - [2] K. Fukushima, B. Mohanty, and N. Xu, (2020), [arXiv:2009.03006 \[hep-ph\]](#).
 - [3] K. Fukushima and C. Sasaki, *Prog. Part. Nucl. Phys.* **72**, 99 (2013), [arXiv:1301.6377 \[hep-ph\]](#).
 - [4] M. Buballa and S. Carignano, *Prog. Part. Nucl. Phys.* **81**, 39 (2015), [arXiv:1406.1367 \[hep-ph\]](#).
 - [5] P. Braun-Munzinger, V. Koch, T. Schäfer, and J. Stachel, *Phys. Rept.* **621**, 76 (2016), [arXiv:1510.00442 \[nucl-th\]](#).
 - [6] C. S. Fischer, *Prog. Part. Nucl. Phys.* **105**, 1 (2019), [arXiv:1810.12938 \[hep-ph\]](#).
 - [7] G. Baym, T. Hatsuda, T. Kojo, P. D. Powell, Y. Song, and T. Takatsuka, *Rept. Prog. Phys.* **81**, 056902 (2018), [arXiv:1707.04966 \[astro-ph.HE\]](#).
 - [8] D. Blaschke and N. Chamel, *Astrophys. Space Sci. Libr.* **457**, 337 (2018), [arXiv:1803.01836 \[nucl-th\]](#).
 - [9] L. McLerran and V. Skokov, *Nucl. Phys. A* **929**, 184 (2014), [arXiv:1305.0774 \[hep-ph\]](#).
 - [10] V. A. Miransky and I. A. Shovkovy, *Phys. Rept.* **576**, 1 (2015), [arXiv:1503.00732 \[hep-ph\]](#).
 - [11] R. Fukuda, K. Fukushima, T. Hayata, and Y. Hidaka, *Phys. Rev. D* **89**, 014508 (2014), [arXiv:1309.3500 \[hep-ph\]](#).
 - [12] T. Brauner, G. Filios, and H. Kolešová, *Phys. Rev. Lett.* **123**, 012001 (2019), [arXiv:1902.07522 \[hep-ph\]](#).
 - [13] G. Basar, G. V. Dunne, and D. E. Kharzeev, *Phys. Rev. Lett.* **104**, 232301 (2010), [arXiv:1003.3464 \[hep-ph\]](#).
 - [14] T. Kojo, Y. Hidaka, L. McLerran, and R. D. Pisarski, *Nucl. Phys. A* **843**, 37 (2010), [arXiv:0912.3800 \[hep-ph\]](#).
 - [15] E. J. Ferrer, V. de la Incera, and A. Sanchez, *Acta Phys. Polon. Supp.* **5**, 679 (2012), [arXiv:1205.4492 \[nucl-th\]](#).
 - [16] E. Nakano and T. Tatsumi, *Phys. Rev. D* **71**, 114006 (2005), [arXiv:hep-ph/0411350](#).
 - [17] T. Takatsuka, K. Tamiya, T. Tatsumi, and R. Tamagaki, *Prog. Theor. Phys.* **59**, 1933 (1978).
 - [18] T. Brauner and N. Yamamoto, *JHEP* **04**, 132 (2017), [arXiv:1609.05213 \[hep-ph\]](#).
 - [19] D. T. Son and M. A. Stephanov, *Phys. Rev. D* **77**, 014021 (2008), [arXiv:0710.1084 \[hep-ph\]](#).

- [20] F. Canfora, S. Carignano, M. Lagos, M. Mannarelli, and A. Vera, *Phys. Rev. D* **103**, 076003 (2021), [arXiv:2012.05921 \[hep-ph\]](#).
- [21] E. J. Ferrer, V. de la Incera, I. Portillo, and M. Quiroz, *Phys. Rev. D* **89**, 085034 (2014), [arXiv:1311.3400 \[nucl-th\]](#).
- [22] E. Witten, *Nucl. Phys. B* **223**, 433 (1983).
- [23] J. Ruostekoski and J. R. Anglin, *Phys. Rev. Lett.* **86**, 3934 (2001).
- [24] E. Witten, *Nucl. Phys. B* **160**, 57 (1979).
- [25] T. H. R. Skyrme, *Proc. Roy. Soc. Lond. A* **260**, 127 (1961).
- [26] I. Zahed and G. E. Brown, *Phys. Rept.* **142**, 1 (1986).
- [27] G. S. Adkins, C. R. Nappi, and E. Witten, *Nucl. Phys. B* **228**, 552 (1983).
- [28] Y.-L. Ma and M. Rho, *Sci. China Phys. Mech. Astron.* **60**, 032001 (2017), [arXiv:1612.06600 \[nucl-th\]](#).
- [29] M. Kawaguchi, Y.-L. Ma, and S. Matsuzaki, *Phys. Rev. C* **100**, 025207 (2019), [arXiv:1810.12880 \[nucl-th\]](#).
- [30] E. Witten, *Nucl. Phys. B* **223**, 422 (1983).
- [31] J. Wess and B. Zumino, *Phys. Lett. B* **37**, 95 (1971).
- [32] G. H. Derrick, *J. Math. Phys.* **5**, 1252 (1964).
- [33] I. R. Klebanov, *Nucl. Phys. B* **262**, 133 (1985).
- [34] K. Nawa, H. Suganuma, and T. Kojo, *Phys. Rev. D* **79**, 026005 (2009), [arXiv:0810.1005 \[hep-th\]](#).